UNIVERSITY OF NIŠ
The scientific journal **FACTA UNIVERSITATIS**
Series: **Mechanics, Automatic Control and Robotics** Vol.2, No 10, 2000 pp. 1329 - 1348
Editor of series: Katica (Stevanovi}) Hedrih, e-mail: katica@masfak.masfak.ni.ac.yu
Address: Univerzitetski trg 2, 18000 Niš, YU, Tel: +381 18 547-095, Fax: +381 18 547-950
http:// ni.ac.yu/Facta

NONLINEAR FINITE ELEMENT ANALYSIS OF R/C SHELLS

UDC 624.074.43:624.041(045)

Demosthenes G. Talaslidis [1], Aristotle Ch. Tokatlidis [2]

[1] Mete Sysm S.A., Th. Sofouli 56, 54655 Thessaloniki, Greece
E-mail: metesysm@otenet.gr
[2] Department of Civil Engineering, Aristotle University, 54006 Thessaloniki, Greece
E-mail: talaslid@civil.auth.gr

Abstract. *The paper focuses on the development and implementation of an appropriate finite element formulation and a macrolevel material model for the efficient and reliable nonlinear analysis of reinforced concrete (R/C) shell structures. Towards this aim, an element formulation is presented based on the Hu-Washizu principle. Independent approximations of displacements (bilinear), strains and stresses (piecewise constant) provide a consistent mechanism for describing the progressive variation of the material properties through the element. Furthermore, re-evaluations of stiffness coefficients and internal forces as well as correction of imbalances at successive increments become very simple, thus leading to a significant reduction of computational effort. The employed material model is based on the assumptions of the "Modified Compression Field Theory". This model in conjunction with a layered approach can in an expedient and economical way predict in a global sense the overall ultimate load behavior. Test examples are analyzed using the proposed approach and comparisons are made with measurements obtained from experimental investigations.*

Key words: *Finite Elements, Nonlinear Analysis, Reinforced Concrete, Shells.*

1. INTRODUCTION

The nonlinear analysis of reinforced concrete shells calls for material models, which are numerically reliable and which describe in a realistic manner the highly nonlinear behavior of the material. Therefore, a reliable macrolevel material model is needed which relies on the results of extensive experimental tests and can predict in a global sense the overall ultimate load behavior of engineering structures. Furthermore, nonlinear finite element analysis demands incremental procedures with the resulting costs of repetitious computations. The accurate description of nonlinear behavior also calls for a finer assembly of elements and further expense. Consequently, simple element formulations

Received May 30, 2000

are needed which can implement the nonlinear material model in an efficient manner. The present paper focuses on the aforementioned aspects of the nonlinear analysis of reinforced concrete shells: development of appropriate finite elements and efficient implementation of nonlinear material models.

The basis of the present finite element formulation is the Hu-Washizu principle[1] with independent approximations of displacements, strains and stresses. The assumptions for these discrete variables follow the proper identification of the element deformational modes and serve to avoid the appearance of superfluous energy and zero energy modes. Furthermore, they incorporate an important modification especially suited for nonlinear analyses: The strain and stresses have piecewise constant approximations. This provides a consistent mechanism for describing the progressive variation of the material properties through the element. Re-evaluations of stiffness coefficients, internal and non-equilibrated forces at successive increments of load become very simple, thus leading to a significant reduction of computational cost [2].

The employed material model is based on the assumptions of the "Modified Compression Field Theory"[3,4]. Stress-strain relationships for plane stress take into consideration nonlinear effects such as cracking and crushing of concrete, tension stiffening, reduction of concrete compressive strength due to transverse tension, yielding and hardening of reinforcing steel. The incremental stress-strain equations are introduced into the proposed plate and shell elements by means of a layered formulation. Test examples are analyzed using the proposed approach and comparisons are made with measurements obtained from experimental investigations.

2. A FINITE ELEMENT APPROXIMATION BASED ON THE HU-WASHIZU PRINCIPLE

2.1. Introduction

A large number of shell element formulations has been proposed in the past [5]. Some of these approaches employ underintegrated elements; other alternatives use stabilization techniques, are based on hybrid/mixed variational principles or include incompatible modes. In the last decade, assumed or enhanced strain formulations have been established. They use enhanced strain modes and many of these formulations are based on generalized principles such as the Hu-Washizu principle. The large variety of the proposed approaches reveals the difficulties facing an element developer seeking to fulfill a series of requirements such as: Avoidance of excessive energy ("locking") and zero energy modes, accurate description of extensional and flexural deformations, insensitivity to mesh distortions, straightforward and efficient extension to nonlinear formulations.

It has been shown [1,6-9] that the use of the Hu-Washizu principle offers a series of advantages and may circumvent most of the aforementioned difficulties. The basis of the present C° formulation is also the Hu-Washizu principle with independent approximations of displacements, strains and stresses. The assumptions for these discrete variables follow the proper identification of the element deformational modes and serve to avoid the appearance of superfluous energy and zero energy modes. Furthermore, they incorporate an important modification especially suited for nonlinear analyses: The strain and stresses have piecewise constant approximations. This approach provides a consistent mechanism for describing the progressive variation of the material properties through the element. Re-

evaluations of stiffness coefficients at successive increments of load require no additional integrations over the elemental area. Additionally, the evaluation of internal forces becomes also very simple and, consequently, the correction of imbalances is readily achieved via the iterative process. Thus, a reduction of computational cost is achieved [2].

2.2. Basic features

The underlying shell theory is formulated in arbitrary curvilinear coordinates and includes the effects of transverse shear strains [10]. The transverse normal stress and the associated work are neglected; the small extension of the normal is also neglected. The corresponding expressions are later specialized to specific geometries.

The basis of the present formulation is the general functional of the Hu-Washizu, which admits independent approximations of displacements, strains and stresses, and provides consistent relations between the discrete parameters. As stationary criteria provide the primitive forms (e.g., equilibrium conditions are expressed in terms of stresses) of the differential and algebraic equations governing the continuum body, the corresponding criteria (i.e., variations of discrete parameters) provide the algebraic versions governing the discrete model. Here, we introduce discrete approximations of each field; these are interrelated through the stationary conditions. Accordingly, the scheme admits independent forms of approximation for the variables, i.e., full compatibility of displacement, strain and stress is not a prerequisite. The requisite "compatibility" is provided by the stationary criteria. The relaxation of compatibility between the fields enables the suppression of unnecessary higher-order terms, avoidance of unwarranted stiffness and, consequently, more rapid convergence.

Essential steps to our approximation are the identification of higher-order terms in the assumptions for strains and stresses and the realization that these reappear in different components of strains/stresses. In the following, the approach is illustrated for the simple case of a rectangular plate element with width (2Λ) and height (2). Towards this aim we employ the bilinear approximations for the vertical displacement w and the rotations α and β of the plate:

$$w = w_0 + w_1 x_1 + w_2 x_2 + w_{12} x_1 x_2 \tag{1}$$

$$\alpha = \alpha_0 + \alpha_1 x_1 + \alpha_2 x_2 + \alpha_{12} x_1 x_2 \qquad \beta = \beta_0 + \beta_1 x_1 + \beta_2 x_2 + \beta_{12} x_1 x_2 \tag{2), (3}$$

These approximations yield 12 degrees of freedom: 3 rigid body motions $(\bar{w}_0, \bar{\omega}_{13}, \bar{\omega}_{23})$, 2 constant bending modes $(\bar{\kappa}_{11}, \bar{\kappa}_{22})$, 1 constant twist mode $(\bar{\kappa}_{12})$, and 2 constant transverse shear modes $(\bar{\gamma}_1, \bar{\gamma}_2)$. The remaining 4 degrees of freedom comprise the higher order deformational modes and impart strain energy. They correspond to bending $(\tilde{\kappa}_{11}, \tilde{\kappa}_{22})$, warping of the mid-surface and relative $(\tilde{w})$ torsion of the top and bottom surface of the plate $(\tilde{t})$. The analytical expressions for the aforementioned modes are given in Table 1.

Exact satisfaction of the strain-displacement relationships yields the following expressions:

$$\kappa_{11} = \alpha_1 + \alpha_{12} x_2 \doteq \bar{\kappa}_{11} + \tilde{\kappa}_{11} x_2 \qquad \kappa_{22} = \beta_2 + \beta_{12} x_1 \doteq \bar{\kappa}_{22} + \tilde{\kappa}_{22} x_1 \tag{4), (5}$$

$$\kappa_{12} = (1/2)(\alpha_2 + \beta_1) + (1/2)\alpha_{12} x_2 + (1/2)\beta_{12} x_2 \doteq \bar{\kappa}_{12} + \underline{(1/2)\tilde{\kappa}_{11} x_1} + \underline{(1/2)\tilde{\kappa}_{22} x_2} \tag{6}$$

$$\begin{aligned}\varepsilon_{13} &= (1/2)(\alpha_0 + \alpha_1 x_1 + \alpha_2 x_2 + \alpha_{12} x_1 x_2) + (1/2)(w_1 + w_{12} x_2) \\ &\doteq \bar{\gamma}_1 + (1/2)(\bar{\kappa}_{12} + \tilde{t} + \tilde{w}) x_2 + \underline{(1/2)\bar{\kappa}_{11} x_1} + \underline{(1/2)\tilde{\kappa}_{11} x_1 x_2}\end{aligned} \tag{7}$$

$$\begin{aligned}\varepsilon_{12} &= (1/2)(\beta_0 + \beta_1 x_1 + \beta_2 x_2 + \beta_{12} x_1 x_2) + (1/2)(w_2 + w_{12} x_1) \\ &\doteq \bar{\gamma}_2 + (1/2)(\bar{\kappa}_{12} - \tilde{t} + \tilde{w}) x_1 + \underline{(1/2)\bar{\kappa}_{22} x_2} + \underline{(1/2)\tilde{\kappa}_{22} x_1 x_2}\end{aligned} \tag{8}$$

	w	α	β
$\bar{w}_0$	w_0	–	–
$\bar{\omega}_{13}$	$-(1/2)w_1 x_1$	$(1/2)\alpha_0$	–
$\bar{\omega}_{23}$	$-(1/2)w_2 x_2$	–	$(1/2)\beta_0$
$\bar{\kappa}_{11}$	–	$\alpha_1 x_1$	–
$\bar{\kappa}_{22}$	–	–	$\beta_2 x_2$
$\bar{\kappa}_{12}$	–	$(1/2)\alpha_2 x_2$	$(1/2)\beta_1 x_1$
$\tilde{\kappa}_{11}$	–	$\alpha_{12} x_1 x_2$	–
$\tilde{\kappa}_{22}$	–	–	$\beta_{12} x_1 x_2$
$\bar{\gamma}_1$	$(1/2)w_1 x_1$	$(1/2)\alpha_0$	–
$\bar{\gamma}_2$	$(1/2)w_2 x_2$	–	$(1/2)\beta_0$
$\tilde{w}$	$w_{12} x_1 x_2$	–	–
$\tilde{t}$	–	$(1/2)\alpha_2 x_2$	$-(1/2)\beta_1 x_1$

Table 1. Rigid body motions and deformational modes of the plate element

The underlined terms containing $\tilde{\kappa}_{11}$ and $\tilde{\kappa}_{22}$ in the expression (6) for the twist mode κ_{12} appear also in the relations (7) and (8) for the transverse shear ε_{13} and ε_{23}. These terms are of higher order; they vanish from the energy density in the *limit*. Still, each must be present *somewhere* in the *finite* element to inhibit that mode; however, it is sufficient to retain such terms in but one of the components. Thus, it is enough to retain these terms either in the expression for κ_{11} and κ_{22} or for κ_{12}. Otherwise, they produce extensive energy, thus leading to "shear locking". The influence of these additional terms can be illustrated, e.g., for the case of a linear rotation field $a = \bar{\phi} x_1$, which corresponds to a constant bending mode. The resulting deformational modes

$$\kappa_{11} = \bar{\phi} \qquad \varepsilon_{13} = \bar{\phi} x_1 \ \ /2 \tag{9}$$

yield the strain energy:

$$\begin{aligned}U = U_B + U_S &= \frac{1}{2}\int_{-1}^{1}\int_{-\Lambda}^{\Lambda} \frac{Et^3}{12(1-\nu^2)} \kappa_{11}^2 dx_1 dx_2 + \frac{1}{2}\int_{-1}^{1}\int_{-\Lambda}^{\Lambda} \frac{Et}{2(1+\nu)} (2\varepsilon_{13})^2 dx_1 dx_2 \\ &= \frac{Et^3 \bar{\phi}^2 \Lambda}{6(1-\nu^2)}\left[1 + 2(1-\nu)\frac{\Lambda^2}{t^2}\right]\end{aligned} \tag{10}$$

The ratio of the produced strain energy to the exact value is

$$\frac{U}{U_{ex}} = 1 + 2(1-\nu)\frac{\Lambda^2}{t^2} \tag{11}$$

It becomes apparent that as $(t \to 0)$ this ratio increases, thus leading to "locking".

The appearance of the constant term $\overline{\kappa}_{12}$ in the expressions (7) and (8) for the transverse shear deserves some attention. In case of a constant twist, the displacement field takes the form $w = \overline{w}x_1x_2$ and the compatible rotations become $\alpha = -\overline{w}x_2$ and $\beta = -\overline{w}x_1$. The combination of these fields produces no excessive energy since the corresponding transverse shear strains are zero:

$$\varepsilon_{13} = \frac{1}{2}(\alpha + w_{,1}) = \frac{1}{2}(-\overline{w}x_2 + \overline{w}x_2) = 0 \tag{12}$$

$$\varepsilon_{23} = \frac{1}{2}(\beta + w_{,2}) = \frac{1}{2}(-\overline{w}x_1 + \overline{w}x_1) = 0 \tag{13}$$

$$\kappa_{12} = \frac{1}{2}(\alpha_{,2} + \beta_{,1}) = \frac{1}{2}(-\overline{w} - \overline{w}) = -\overline{w} \tag{14}$$

Summarizing, the flaw in the formulation is a result of the exact satisfaction of the strain-displacement relationships. Contrary, locking is prevented if the strain assumptions employed using the Hu-Washizu principle do not contain the underlined terms of eqs. (6) to (8). The remaining terms sufficiently describe the element deformation modes and suppress zero energy modes. This becomes apparent if the displacement/rotation fields are expressed in the form:

$$w = \overline{w}_0 + (-\overline{\omega}_{13} + \overline{\gamma}_1)x_1 + (-\overline{\omega}_{23} + \overline{\gamma}_2)x_2 + \underline{\widetilde{w}x_1x_2} \tag{15}$$

$$\alpha = (\overline{\omega}_{13} + \overline{\gamma}_1) + \overline{\kappa}_{11}x_1 + (\overline{\kappa}_{12} + \underline{\widetilde{t}})x_2 + \underline{\widetilde{\kappa}_{11}x_1x_2} \tag{16}$$

$$\beta = (\overline{\omega}_{23} + \overline{\gamma}_2) + (\overline{\kappa}_{12} - \underline{\widetilde{t}})x_1 + \overline{\kappa}_{22}x_2 + \underline{\widetilde{\kappa}_{22}x_1x_2} \tag{17}$$

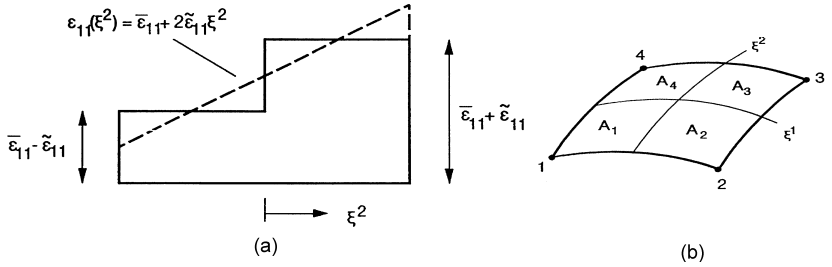

Fig.1. (a) Piecewise constant approximations for strains and stresses
(b) Subdomains and areas

2.3. Discretization

The ideas presented in Section 2.2 suggest a linear variation in the ξ^2-direction for the approximation of the strains $(\varepsilon_{11}, \kappa_{11}, \gamma_1)$, a linear variation in the ξ^1-direction for the

strains ($\varepsilon_{22},\kappa_{22},\gamma_2$), and a constant approximation for ($\varepsilon_{12},\kappa_{12}$). However, the formulation can be further simplified if the linear variation of the strains and of the corresponding stresses is replaced by a piecewise constant approximation (Fig. 1a). Introducing the four subdomains of Fig. 1b we have the following discrete parameters for the strains

$$\varepsilon_{11}=\begin{cases}\varepsilon_{11}^{A} & \text{in } A_1+A_2\\ \varepsilon_{11}^{B} & \text{in } A_3+A_4\end{cases}\qquad \varepsilon_{22}=\begin{cases}\varepsilon_{22}^{C} & \text{in } A_1+A_4\\ \varepsilon_{22}^{D} & \text{in } A_2+A_3\end{cases}\qquad \varepsilon_{12}=\bar{\varepsilon}_{12} \tag{18}$$

$$\kappa_{11}=\begin{cases}\kappa_{11}^{A} & \text{in } A_1+A_2\\ \kappa_{11}^{B} & \text{in } A_3+A_4\end{cases}\qquad \kappa_{22}=\begin{cases}\kappa_{22}^{C} & \text{in } A_1+A_4\\ \kappa_{22}^{D} & \text{in } A_2+A_3\end{cases}\qquad \kappa_{12}=\bar{\kappa}_{12} \tag{19}$$

$$\gamma_1=\begin{cases}\gamma_1^{A} & \text{in } A_1+A_2\\ \gamma_1^{B} & \text{in } A_3+A_4\end{cases}\qquad \gamma_2=\begin{cases}\gamma_2^{C} & \text{in } A_1+A_4\\ \gamma_2^{D} & \text{in } A_2+A_3\end{cases} \tag{20}$$

Using the piecewise constant parameters for the strains and stresses and the bilinear approximations for the displacement/rotation fields the Hu-Washizu principle yealds

$$\begin{aligned}\Pi_{HW}=&\frac{1}{2}\bar{\boldsymbol{\varepsilon}}^T\bar{\boldsymbol{D}}_E\bar{\boldsymbol{\varepsilon}}+\frac{1}{2}\bar{\boldsymbol{\kappa}}^T\bar{\boldsymbol{D}}_B\bar{\boldsymbol{\kappa}}+\frac{1}{2}\bar{\boldsymbol{\gamma}}^T\bar{\boldsymbol{D}}_S\bar{\boldsymbol{\gamma}}-\frac{1}{2}(\boldsymbol{N}^T\boldsymbol{A}_N\bar{\boldsymbol{\varepsilon}}+\bar{\boldsymbol{\varepsilon}}^T\boldsymbol{A}_N\boldsymbol{N})\\ &-\frac{1}{2}(\boldsymbol{M}^T\boldsymbol{A}_M\bar{\boldsymbol{\kappa}}+\bar{\boldsymbol{\kappa}}^T\boldsymbol{A}_M\boldsymbol{M})-\frac{1}{2}(\boldsymbol{Q}^T\boldsymbol{A}_Q\bar{\boldsymbol{\gamma}}+\bar{\boldsymbol{\gamma}}^T\boldsymbol{A}_Q\boldsymbol{Q})+\frac{1}{2}(\boldsymbol{N}^T\boldsymbol{B}_{\mathrm{E}}\boldsymbol{u}+\boldsymbol{u}^T\boldsymbol{B}_E\boldsymbol{N})\\ &+\frac{1}{2}(\boldsymbol{M}^T\boldsymbol{B}_B\boldsymbol{u}+\boldsymbol{u}^T\boldsymbol{B}_B\boldsymbol{M})+\frac{1}{2}(\boldsymbol{Q}^T\boldsymbol{B}_S\boldsymbol{u}+\boldsymbol{u}^T\boldsymbol{B}_S\boldsymbol{Q})-\boldsymbol{u}^T\boldsymbol{p}\end{aligned} \tag{22}$$

In relationship (22) ($\boldsymbol{N},\boldsymbol{M},\boldsymbol{Q}$) and ($\bar{\boldsymbol{\varepsilon}},\bar{\boldsymbol{\kappa}},\bar{\boldsymbol{\gamma}}$) contain the discrete parameters for the stresses and strains, respectively:

$$\begin{gathered}\boldsymbol{N}^T=\begin{bmatrix} n_A^{11} n_B^{11} & n_C^{22} & n_D^{22} & \bar{n}^{12}\end{bmatrix},\quad \boldsymbol{M}^T=\begin{bmatrix} m_A^{11} & m_B^{11} & m_C^{22} & m_D^{22} & \bar{m}^{12}\end{bmatrix},\\ \boldsymbol{Q}^T=\begin{bmatrix} q_A^1 & q_B^1 & q_C^2 & q_D^2\end{bmatrix}\\ \bar{\boldsymbol{\varepsilon}}^T=\begin{bmatrix} \varepsilon_{11}^A & \varepsilon_{11}^B & \varepsilon_{22}^C & \varepsilon_{22}^D & 2\bar{\varepsilon}_{12}\end{bmatrix},\quad \bar{\boldsymbol{\kappa}}^T=\begin{bmatrix} \kappa_{11}^A & \kappa_{11}^B & \kappa_{22}^C & \kappa_{22}^D & 2\bar{\kappa}_{12}\end{bmatrix},\\ \bar{\boldsymbol{\gamma}}^T=\begin{bmatrix} \gamma_1^A & \gamma_1^B & \gamma_2{}^C & \gamma_2^D\end{bmatrix}\end{gathered} \tag{23)-(28}$$

The diagonal matrices ($\boldsymbol{A}_N,\boldsymbol{A}_M,\boldsymbol{A}_Q$) contain only the areas of the subdomains. The discretized elasticity matrices ($\boldsymbol{D}_E,\boldsymbol{D}_B,\boldsymbol{D}_S$) take the forms

$$\overline{\boldsymbol{D}}_E = \frac{Et}{1-\nu^2}\begin{bmatrix} A_1+A_2 & 0 & \nu A_1 & \nu A_2 & 0 \\ & A_3+A_4 & \nu A_4 & \nu A_3 & 0 \\ & & A_1+A_4 & 0 & 0 \\ & sym. & & A_2+A_3 & 0 \\ & & & & \dfrac{1-\nu}{2}A \end{bmatrix} \tag{29}$$

$$\overline{\boldsymbol{D}}_E = \frac{t^2}{12}\overline{\boldsymbol{D}}_E \qquad \overline{\boldsymbol{D}}_S = \frac{Et}{2\kappa_Q(1+\nu)}\begin{bmatrix} A_1+A_2 & & & \mathbf{0} \\ & A_3+A_4 & & \\ & & A_1+A_4 & \\ \mathbf{0} & & & A_2+A_3 \end{bmatrix} \tag{30), (31}$$

Variation of the stress resultants $(\delta \boldsymbol{N}^T, \delta \boldsymbol{M}^T, \delta \boldsymbol{Q}^T)$ leads to the discrete strain-displacement relationships.

$$\overline{\boldsymbol{\varepsilon}} = \boldsymbol{A}_N^{-1}\boldsymbol{B}_E\boldsymbol{u} \qquad \overline{\boldsymbol{\kappa}} = \boldsymbol{A}_M^{-1}\boldsymbol{B}_B\boldsymbol{u} \qquad \overline{\boldsymbol{\gamma}} = \boldsymbol{A}_Q^{-1}\boldsymbol{B}_S\boldsymbol{u} \tag{32}$$

$$\boldsymbol{u}^T = \begin{bmatrix} \boldsymbol{u}^1 & \boldsymbol{u}^2 & \boldsymbol{u}^3 & \boldsymbol{u}^4 \end{bmatrix} \qquad \boldsymbol{u}^\kappa = \begin{bmatrix} u_1^\kappa & u_2^\kappa & \phi_1^\kappa & \phi_2^\kappa \end{bmatrix} \tag{33}$$

Variation of the strain parameters $(\delta\overline{\boldsymbol{\varepsilon}}^T, \delta\overline{\boldsymbol{\kappa}}^T, \delta\overline{\boldsymbol{\gamma}}^T)$ yields the discrete constitutive equations

$$\boldsymbol{N} = \boldsymbol{A}_N^{-1}\overline{\boldsymbol{D}}_E\overline{\boldsymbol{\varepsilon}} \qquad \boldsymbol{M} = \boldsymbol{A}_M^{-1}\overline{\boldsymbol{D}}_B\overline{\boldsymbol{\kappa}} \qquad \boldsymbol{Q} = \boldsymbol{A}_Q^{-1}\overline{\boldsymbol{D}}_S\overline{\boldsymbol{\gamma}} \tag{34}$$

Finally, varying the nodal displacements/rotations the discrete form of the equilibrium equations is obtained.

$$\boldsymbol{B}_E^T\boldsymbol{N} + \boldsymbol{B}_B^T\boldsymbol{M} + \boldsymbol{B}_S^T\boldsymbol{Q} = \boldsymbol{p} \tag{35}$$

Substituting relationships (32) to (34) into (35) we obtain the stiffness matrix for the element. The implementation of the material model for the reinforced concrete will be described in Section 3.

Some features of the proposed approximation are noteworthy: (i) the variational principle provides consistent relationships between all discrete variables; (ii) the independent approximation of strains and stresses allows the straightforward representation of constant and higher order deformation modes: the homogeneous strains are augmented by specific terms that are introduced to accommodate deformational modes of higher order; (iii) the omission of superfluous higher order terms reduces the internal energy; no excessive energy (locking) is present; (iv) the evaluation of the coefficients of the stiffness matrix requires very simple operations, no numerical integrations or inversions; (v) a displacement formulation can be achieved on the element level without inversions. This leads to symmetric and positive definite matrices with all the desirable advantages; (vi) the effects of extensional and flexural behavior are represented by comparable approximations.

The concept of piecewise constant approximations is especially suited for the nonlinear analysis of reinforced concrete shells: (i) the piecewise constant stresses/strains provide a consistent mechanism for describing the progressive variation of the material

properties through the element; (ii) the subdomain concept is consistent with the assumptions of the material model; (iii) re-evaluations of stiffness coefficients at successive increments of load require no additional integrations over the elemental area; (iv) the evaluation of internal forces is very simple and, consequently, the correction of imbalances is readily achieved via the iterative process, thus resulting to a reduction of computational effort.

3. MATERIAL MODEL FOR REINFORCED CONCRETE

3.1. Introduction

In the past, a large number of more or less sophisticated material models for concrete and for the interface between concrete and steel have been proposed. However, there exists no generally accepted constitutive law and there is a discrepancy between sophisticated nonlinear analysis and structural engineering practice. In the following, a review of established models is presented and remarks concerning their suitability for a finite element analysis are made. The proposed model is described as well as its implementation in the finite element formulation presented in Section 2.

Non-linear elastic models [12] treat biaxially stressed concrete as an orthotropic material. Coefficients of the material stiffness matrix are expressed in terms of stress and strain invariants[11] or stem from equivalent uniaxial relations referred to the principle axes of orthotropy. These models are simple and applicable in a straightforward manner. However, the principal directions of stresses and strains are required to coincide in order to preserve invariance of the constitutive tensor [13].

Constitutive models based on the *theory of plasticity* [14] have been also employed to describe the irrecoverable part of the nonlinear deformations of concrete. Plasticity based models require the definition in the stress space of a yield surface, a failure surface, and intermediate loading surfaces. Finally, the incremental stress-strain relationships are formulated by applying the flow rule. Although these models have a firm theoretical basis they are more complicated than non-linear elastic models. Furthermore, deviations have been observed in cases of inelastic volume changes near the failure load. *Plastic-fracture* [15] and *endochronic* [16] constitutive models can be regarded as extensions of elastoplastic models. These models offer an enhanced capability in describing the post-peak response or the response to complex cyclic loadings. However, the complicated nature of these models imposes difficulties in numerical applications.

Discrete crack models[17] account for the displacement discontinuity across the crack. These models require a high computational effort, lead to complexities in element formulations and are unsuitable for the analysis of reinforced concrete plates and shells [18].

In *smeared crack models* the cracked structure is treated as a continuum. The effects of cracking are taken into account by appropriate modifications of the stress-strain relations. According to *fixed orthogonal crack models*, the orientation of the crack in an element is defined by the direction of the principal tensile stress that initially exceeds the tensile strength of concrete. Cracked concrete is treated as an orthotropic material. The orientation of the axes of orthotropy is kept constant upon subsequent loading stages. New cracks are allowed to propagate in a direction perpendicular to the length of the

existing ones. However, in cases of anisotropic reinforcement or non-proportional loading the principal axes rotate and fixed crack models overestimate the failure load. In *fixed non-orthogonal crack models* [19] additional cracks are allowed to appear in directions not orthogonal to the orientation of the existing ones, when the change in the direction of principal axes exceeds a predefined threshold angle. The formulation avoids deficiencies of the fixed crack concept. Nevertheless, numerical implementation of the model is rather complicated. Furthermore, the use of an inappropriate finite element formulation may cause numerical problems (zero energy modes). *Rotating crack models* [20,21] allow for the change in direction of cracks within a load increment. Only the most recent cracks parallel to the actual principal axes are taken into account. Rotating crack models are computationally efficient and consistent with experimental evidence. Recently, smeared crack models based on the theory of plasticity have been also proposed [22]. They are characterized by a Rankine yield criterion with an appropriate softening law.

3.2. Reinforced concrete model-Implementation

A reliable but not too complicated material model for plane stress conditions is a prerequisite for the realistic finite element analysis of reinforced concrete plates and shells. Extension of the two-dimensional model to the general case of a shell can be achieved in a straightforward manner by means of a layered formulation. The proposed approach is based on the "Modified Compression Field Theory", which was developed by Collins and co-workers in order to investigate the biaxial behavior of reinforced concrete [3-4, 20, 23-24].

According to the "Modified Compression Field Theory", cracked concrete is treated as a new material with its own stress-strain characteristics. Constitutive relations stem from experimental investigations of biaxially loaded reinforced concrete specimens [3]. Orthogonally reinforced concrete specimens were subjected to various combinations of monotonic loading such as pure shear, uniaxial compression, combined shear and biaxial tension or compression as well as to different ratios of shear to axial forces. Experimental measurements served as a basis to formulate stress-strain relations for uncracked and cracked concrete.

In determining the behavioral characteristics of reinforced concrete, stresses and strains are considered in terms of average values when taken over areas large enough to include several cracks. It is assumed that steel reinforcement is distributed over the entire element, while concrete and steel bars are perfectly bounded together undergoing equal strains. An essential assumption for developing the model according to the "Modified Compression Field Theory" is that the principal directions of average concrete stresses coincide with the principal directions of average concrete strains at every loading stage. Experimental testing has shown that the directions of principal stresses deviate somewhat from the directions of principal strains, especially in the case of high compressive stresses. However, it remains a reasonable simplification to assume that the principal axes of stress and strain co-rotate.

The stress-strain relationships for concrete are referred to the directions of the principal stresses (or strains). The principal compressive stress in concrete σ_{c2} is a function of the principal compressive strain ε_2 but also depends on the principal tensile strain ε_1. Co-existing tension in the transverse direction has a softening effect on the peak compressive stress of concrete f_p. The proposed stress-strain curve for concrete under

compression is a parabola:

$$\sigma_{c2} = f_P\left[2\left(\frac{\varepsilon_2}{\varepsilon_0}\right)-\left(\frac{\varepsilon_2}{\varepsilon_0}\right)^2\right] \quad \text{for} \quad 0 \geq \varepsilon_2 \geq 1.5\varepsilon_0 \tag{36}$$

$$\sigma_{c2} = 0 \quad \text{for} \quad 1.5\varepsilon_0 > \varepsilon_2 \tag{37}$$

with

$$f_p = \frac{f_c}{0.8 - 0.34(\varepsilon_1 / \varepsilon_0)} \leq f_c \tag{38}$$

In relationship (38) f_c is the cylinder compressive strength and ε_0 is the cylinder strain corresponding to f_c. Note that as ε_0 is a negative quantity, increasing tensile strain ε_1 will reduce peak strength f_p. The ultimate compressive strain of concrete is taken equal to $1.5\varepsilon_0$. For higher strains, concrete is assumed to resist no stresses due to crushing failure.

Uncracked concrete is assumed to behave as a linear elastic material. The relationship between the principal tensile stress σ_{c1} and principal tensile strain ε_1 prior to cracking is given by

$$\sigma_{c1} = E_{c0}\varepsilon_1 \quad 0 < \varepsilon_1 \leq \varepsilon_{ct} \quad \varepsilon_{cr} = f_{ct} / E_{c0} \tag{39}$$

The initial value for the tangential modulus of elasticity is taken to be

$$E_{c0} = 2f_c / \varepsilon_0 \tag{40}$$

For the concrete tensile strength a relationship is adopted given in Eurocode 2 [24]:

$$f_{ct} = 0.3\sqrt[3]{f_c^2} \tag{41}$$

The behavior of cracked concrete under tension is described by a descending branch in the stress-strain diagram. The decaying function in the post-cracked region accounts for the tension stiffening effect and is given by

$$\sigma_{c1} = f_a /(1 + \sqrt{200\varepsilon_1}) \tag{42}$$

The tension stiffening mechanism develops as bond between steel and concrete allows the transmission of tensile stresses from the reinforcement to the intact regions of concrete between cracks. Once the reinforcement begins to yield, its ability to transfer stresses is reduced and average tensile stresses of cracked concrete are close to zero. Thus, a bound should be imposed on the tension transfer capacity of reinforcement. If there are N layers of steel at a concrete element, then a restraint for the concrete tension stiffening stresses can be formulated as follows:

$$\sigma_{c1} \leq \sum_{i=1}^{N} \rho_i (f_{yi} - \sigma_{si}) \cos^2 \theta_i \tag{43}$$

In eq. (43), ρ_i is the reinforcement ratio for the i^{th} layer, f_{yi} and σ_{si} are yield stress and existing stress, respectively, and θ_i is the angle between the principal tensile stress and the bar direction.

Constitutive equations (36) to (39) and (42) are incorporated into the proposed finite element formulation in order to construct an incremental nonlinear elastic rotating crack

model for reinforced concrete. Uncracked concrete is assumed to be an isotropic, nonlinearly elastic material. The incremental biaxial stress-strain relationships with respect to a cartesian coordinate system is given by

$$\begin{bmatrix} d\sigma_x \\ d\sigma_y \\ d\tau_{xy} \end{bmatrix} = \frac{E_t}{1-v^2} \begin{bmatrix} 1 & v & 0 \\ v & 1 & 0 \\ 0 & 0 & \frac{1-v}{2} \end{bmatrix} \begin{bmatrix} d\varepsilon_x \\ d\varepsilon_y \\ dy_{xy} \end{bmatrix} \tag{44}$$

For the first load increment, the tangential elastic modulus E_t is taken equal to E_{c0} . For subsequent load stages, the tangent moduli in the principal directions are evaluated by differentiating the constitutive equations:

$$E_{ta} = \frac{2f_c}{\varepsilon_0}\left(1 - \frac{\varepsilon_a}{\varepsilon_0}\right), \quad f_c \le \sigma_{ca} \le 0 \qquad a = 1,2 \tag{45}$$

$$E_{ta} = E_{c0}\,, \quad 0 \le \sigma_{ca} \le f_{ct} \tag{46}$$

$$E_{t1} = E_{c0}\,, \quad 0 \le \sigma_{c1} \le f_{ct} \quad \text{and} \quad f_c \le \sigma_{c2} \le 0 \tag{47}$$

$$E_{t2} = \frac{2f_p}{\varepsilon_0}\left(1 - \frac{\varepsilon_2}{\varepsilon_0}\right) \tag{48}$$

where $f_p = f_c/\beta$, and $\beta = 0{,}8 - 0.34(\varepsilon_1/\varepsilon_0) \ge 1$. A uniform elastic module is finally calculated using a weighted average value of E_{t1} and E_{t2} .

$$E_t = \frac{E_{t1}\,|\,\sigma_{c1}\,| + E_{t2}\,|\,\sigma_{c2}\,|}{|\,\sigma_{c1}\,| + |\,\sigma_{c2}\,|} \tag{49}$$

Poisson's ratio for uncracked concrete is assumed constant and equal to 0.20.

Cracking is assumed to occur when the maximum principal tensile stress exceeds the tensile strength of concrete. The direction of the crack or, more precisely, of the "smeared crack field" is considered to be normal to the direction of this stress. In many cases, the principal directions do not remain fixed during successive load increments. Hence, crack inclination changes, co-rotating with the principal strain axes. The proposed approach also accounts for the formulation of orthogonal cracks in two directions.

Cracked concrete is considered to be an orthotropic material with the axes of orthotropy parallel and normal to the crack. Poisson's ratio is set to zero when cracking is initiated. The incremental stress-strain relations are expressed in the reference system of the principal axes as follows:

$$\begin{bmatrix} d\sigma_{c1} \\ d\sigma_{c2} \\ d\tau_{c12} \end{bmatrix} = \begin{bmatrix} \frac{\partial\sigma_{c1}}{\partial\varepsilon_1} & \frac{\partial\sigma_{c1}}{\partial\varepsilon_2} & 0 \\ \frac{\partial\sigma_{c2}}{\partial\varepsilon_1} & \frac{\partial\sigma_{c2}}{\partial\varepsilon_2} & 0 \\ 0 & 0 & \frac{\sigma_{c1} - \sigma_{c2}}{2(\varepsilon_1 - \varepsilon_2)} \end{bmatrix} \begin{bmatrix} d\varepsilon_1 \\ d\varepsilon_2 \\ d\gamma_{12} \end{bmatrix} \tag{50}$$

In a more concise form, eq. (50) can be written as

$$d\boldsymbol{\sigma}_{12} = \boldsymbol{D}_{c12} d\boldsymbol{\varepsilon}_{12} \tag{51}$$

The coefficients of the incremental constitutive matrix $\boldsymbol{D}_{c12}$ are computed by differentiating eqs. (36) to (39) and (42). The diagonal term $\boldsymbol{D}_{c12}(3,3) = (\sigma_{c1} - \sigma_{c2})/2(\varepsilon_1 - \varepsilon_2)$ accounts for the continuously varying tangential shear stiffness of concrete parallel to the crack. The presence of this term is implicit to the "Modified Compression Field Theory" and stems from the basic assumption that the principal concrete stress direction equals the principal concrete strain direction [20]. The term $(\partial\sigma_{c1}/\partial\varepsilon_2)$ is equal to zero, while $(\partial\sigma_{c2}/\partial\varepsilon_1)$ is usually non-zero as a result of the degradation of the compressive strength due to the co-existing transverse tensile strain. The resulting non-symmetry of the stiffness matrix is a significant drawback to the applicability of the model since most finite element programs use an equation solver for symmetric matrices. In the present study, the non-symmetric term $\boldsymbol{D}_{c12}(2,1)$ is neglected. The omission of this term has been found to affect the convergence rate of the nonlinear algorithm but not the final converged solution.

After crack formation, the average concrete stress in the direction normal to the crack decays according to eq. (42) and the diagonal term $(\partial\sigma_{c1}/\partial\varepsilon_2)$ becomes negative. In order to avoid numerical instabilities, a small positive value equal to $0.001E_{c0}$ is employed for calculating stiffness matrix coefficients. The resulting error is eliminated during the iterative procedure, since the actual $\sigma - \varepsilon$ diagram is used for the calculation of the total stress. A similar technique is applied for the softening branch of concrete under compression. The tangential constitutive matrix $\boldsymbol{D}_{c12}$ is referred to a cartesian system by means of a rotational transformation

$$\mathrm{D}_{cxy} = \boldsymbol{T}^T \boldsymbol{D}_{c12} \boldsymbol{T} \qquad \boldsymbol{T} = \begin{bmatrix} \cos^2\theta & \sin^2\theta & \sin 2\theta/2 \\ \sin^2\theta & \cos^2\theta & -\sin 2\theta/2 \\ -\sin 2\theta & \sin 2\theta & \cos^2\theta - \sin^2\theta \end{bmatrix} \tag{52), (53}$$

In eq. (53), θ is the angle between the principal tensile stress direction and the x-axis.

In the proposed formulation steel reinforcement is taken into account by means of a smeared model. Reinforcement bars are uniformly distributed over the mid-surface of the plane stress element. This approach offers significant advantages over discrete reinforcement models, especially when conducting global analyses of large-scale structures. The nonlinear behavior of reinforcing steel is described by a uniaxial elastoplastic stress-strain curve with or without hardening, identical in tension and compression. The dowel action is neglected and the bond between concrete and steel is assumed to remain perfect. The incremental constitutive matrix for the i^{th} steel layer in the local system can be written as

$$\boldsymbol{D}_{sli} = \begin{bmatrix} \rho_i E_i & 0 & 0 \\ 0 & 0 & 0 \\ 0 & 0 & 0 \end{bmatrix} \tag{54}$$

where ρ_i is the reinforcement ratio and E_i is the elastic or plastic modulus for steel

$$E_i = \begin{cases} E_s & |\varepsilon_s| \le |\varepsilon_{sy}| \\ E_{sp} & |\varepsilon_{sy}| < |\varepsilon_s| \le |\varepsilon_{su}| \\ 0 & |\varepsilon_{su}| < |\varepsilon_s| \end{cases} \tag{55}$$

The constitutive matrix $\boldsymbol{D}_{sli}$ is transformed to the global reference system by means of a rotational transformation

$$\mathrm{D}_{sxyi} = \boldsymbol{T}_i^T \boldsymbol{D}_{sli} \boldsymbol{T}_i \tag{56}$$

where $\boldsymbol{T}_i$ is the transformation matrix given by eq. (53).

The total incremental material stiffness matrix for a R/C plane stress element is derived by summing the component matrices for concrete and steel:

$$\boldsymbol{D} = \boldsymbol{D}_{cxy} + \sum_{i=1}^{N} \boldsymbol{D}_{sxyi} \tag{57}$$

3.3. Layered formulation

The incremental stress-strain equations are implemented in the proposed finite element by means of a layered formulation. The finite element is subdivided across its thickness into a number of concrete layers. Each layer is assumed to be in a state of plane stress, while stresses across the thickness of a single layer are considered to be constant. In a similar manner, reinforcing steel is modeled by means of fictitious steel layers. The nonlinear material behavior in each concrete or steel layer is determined by the incremental constitutive equations of the previous section. Since the effect of transverse shear strains in thin shells is small, their influence on the biaxial behavior is neglected.

In order to obtain the constitutive equations for the layered element, we assume for the extensional and flexural strains

$$\dot{\varepsilon}_{\alpha\beta} = {}_0\dot{\varepsilon}_{\alpha\beta} + \theta^3 \dot{\kappa}_{\alpha\beta}, \quad \alpha,\beta = 1,2 \tag{58}$$

while a parabolic variation through the element thickness is adopted for the out of plane shear strains:

$$2\dot{\varepsilon}_{\alpha 3} = \dot{\gamma}_\alpha \left[1 - \left(\frac{2\theta^3}{t} \right)^2 \right] \tag{59}$$

The variables $\dot{\varepsilon}_{\alpha\beta}$, $\dot{\kappa}_{\alpha\beta}$ and $\dot{\gamma}_\alpha$ denote the incremental extensional, bending and transverse shear strains of the element's mid-surface, respectively. The incremental stress-strain relations in each concrete layer are given by

$$\dot{\boldsymbol{\sigma}}_L = \boldsymbol{C} \cdot \dot{\varepsilon}_L \tag{60}$$

where $\dot{\boldsymbol{\sigma}}_L$ and $\dot{\varepsilon}_L$ are the incremental stress and strain matrices for the layer, respectively

$$\dot{\boldsymbol{\sigma}}_{\boldsymbol{L}}^{\boldsymbol{T}} = \begin{bmatrix} \dot{\sigma}^{11} & \dot{\sigma}^{22} & \dot{\sigma}^{12} & \dot{\sigma}^{13} & \dot{\sigma}^{23} \end{bmatrix} \tag{61}$$

$$\dot{\boldsymbol{\varepsilon}}_{\boldsymbol{L}}^{\boldsymbol{T}} = \begin{bmatrix} \dot{\varepsilon}_{11} & \dot{\varepsilon}_{22} & 2\dot{\varepsilon}_{12} & 2\dot{\varepsilon}_{13} & 2\dot{\varepsilon}_{23} \end{bmatrix} \tag{62}$$

By assuming that the transverse shear $\dot{\boldsymbol{\varepsilon}}_{\alpha 3}$ does not affect the in-plane behavior of concrete, the material matrix $\boldsymbol{C}$ is decomposed as follows

$$\boldsymbol{C} = \begin{bmatrix} \boldsymbol{C_E} & \boldsymbol{0} \\ \boldsymbol{0} & \boldsymbol{C_S} \end{bmatrix} \tag{63}$$

$\boldsymbol{C_E}$ is a (3×3)-submatrix accounting for the biaxial nonlinear material behavior within the concrete layer. The (2×2)-matrix $\boldsymbol{C_S}$ represents the transverse shear stress-strain relations, which are assumed to remain linear during load incrementation

$$\boldsymbol{C_S} = \frac{E_{c0}}{2(1+\nu)} \begin{bmatrix} 1 & 0 \\ 0 & 1 \end{bmatrix} \tag{64}$$

The strain energy per unit area of the elements mid-surface is given by the expression

$$U(\dot{\varepsilon}_L) = \frac{1}{2} \int_{-tl2}^{+tl2} \dot{\boldsymbol{\varepsilon}}_L^T \boldsymbol{C} \dot{\boldsymbol{\varepsilon}}_L d\theta^3 \tag{65}$$

Substituting eqs. (58) and (59) into eq.(65) yields an expression for the strain energy in terms of the mid-surface strains

$$U(\dot{\varepsilon}) = \dot{\boldsymbol{\varepsilon}}^T \boldsymbol{E}^c \dot{\boldsymbol{\varepsilon}} / 2 \tag{66}$$

whereas $\dot{\boldsymbol{\varepsilon}}$ is the vector of incremental mid-surface strains

$$\dot{\boldsymbol{\varepsilon}}_{\boldsymbol{L}}^{\boldsymbol{T}} = \begin{bmatrix} {}_0\dot{\varepsilon}_{11} & {}_0\dot{\varepsilon}_{22} & 2{}_0\dot{\varepsilon}_{12} & \dot{\kappa}_{11} & \dot{\kappa}_{22} & 2\dot{\kappa}_{12} & \dot{\gamma}_1 & \dot{\gamma}_2 \end{bmatrix} \tag{67}$$

and $\boldsymbol{E}^c$ is a constitutive matrix of the form

$$\boldsymbol{E}^c = \begin{bmatrix} \boldsymbol{E}_{00}^{\boldsymbol{c}} & \boldsymbol{E}_{01}^{\boldsymbol{c}} & \boldsymbol{0} \\ & \boldsymbol{E}_{11}^{\boldsymbol{c}} & \boldsymbol{0} \\ sym & & \boldsymbol{E}_{33}^{\boldsymbol{c}} \end{bmatrix}, \quad \boldsymbol{E}_{00}^{\boldsymbol{c}} = \int_{-tl2}^{+tl2} \boldsymbol{C_E} d\theta^3, \quad \boldsymbol{E}_{01}^{\boldsymbol{c}} = \int_{-tl2}^{+tl2} \theta^3 \boldsymbol{C_E} d\theta^3 \quad \boldsymbol{E}_{11}^{\boldsymbol{c}} = \int_{-tl2}^{+tl2} (\theta^3)^2 \boldsymbol{C_E} d\theta^3 \tag{68)-(71}$$

$$\boldsymbol{E}_{33}^{\boldsymbol{c}} = \int_{-tl2}^{+tl2} f(\theta^3) \boldsymbol{C_S} d\theta^3, \quad f(\theta^3) = 1 - \left(\frac{2\theta^3}{t} \right)^2 \tag{72}$$

Evaluation of the coefficients of the stiffness matrix requires integration in the direction of thickness. The proposed element is subdivided into 9 concrete layers of constant thickness and the trapezoidal Simpson integration rule is employed.

In the general case, material properties vary through the element thickness and symmetry about the middle surface $\theta^3 = 0$ is not preserved. As a result, coupling is

introduced between extensional and flexural strains ($\boldsymbol{E}_{01}^{c} \neq \mathbf{0}$). The implication of this coupling is that, even for plate bending problems, in-plane boundary conditions must be specified for a complete description of the problem.

A similar procedure is followed in order to evaluate the constitutive matrix $\mathbf{E}^{\mathbf{S}}$ for the reinforcing steel. If an element is reinforced with N steel layers, then the following relations hold

$$\boldsymbol{E}^{s} = \begin{bmatrix} \boldsymbol{E}_{00}^{s} & \boldsymbol{E}_{01}^{s} & \mathbf{0} \\ & \boldsymbol{E}_{11}^{s} & \mathbf{0} \\ sym & & \mathbf{0} \end{bmatrix} \tag{73}$$

$$\boldsymbol{E}_{00}^{s} = \sum_{i=1}^{N} \boldsymbol{D}_{sxyi} \qquad \boldsymbol{E}_{01}^{s} = \sum_{i=1}^{N} \theta_{i}^{3} \boldsymbol{D}_{sxyi} \qquad \boldsymbol{E}_{11}^{s} = \sum_{i=1}^{N} (\theta_{i}^{3})^{2} \boldsymbol{D}_{sxyi} \tag{74}$$

The total material stiffness matrix is the sum of the two constituent matrices $\boldsymbol{E}^{c}$ and $\boldsymbol{E}^{S}$.

$$\boldsymbol{E} = \boldsymbol{E}^{c} + \boldsymbol{E}^{s} \tag{75}$$

The expression for the strain energy per unit area becomes

$$U = \frac{1}{2}({}_{0}\dot{\boldsymbol{\varepsilon}}^{T} \boldsymbol{E}_{\mathbf{00}} {}_{0}\dot{\boldsymbol{\varepsilon}} + \dot{\boldsymbol{\kappa}}^{T} \boldsymbol{E}_{\mathbf{11}} \dot{\boldsymbol{\kappa}} + \dot{\boldsymbol{\gamma}}^{T} \boldsymbol{E}_{\mathbf{33}} \dot{\boldsymbol{\gamma}} + {}_{0}\dot{\boldsymbol{\varepsilon}}^{T} \boldsymbol{E}_{\mathbf{01}} \dot{\boldsymbol{\kappa}} + \dot{\boldsymbol{\kappa}}^{T} \boldsymbol{E}_{\mathbf{10}} {}_{0}\dot{\boldsymbol{\varepsilon}}) \tag{76}$$

where

$${}_{0}\dot{\boldsymbol{\varepsilon}} = \begin{bmatrix} {}_{0}\dot{\varepsilon}_{11} & {}_{0}\dot{\varepsilon}_{22} & 2{}_{0}\dot{\varepsilon}_{12} \end{bmatrix} \quad \dot{\boldsymbol{\kappa}} = \begin{bmatrix} \dot{\kappa}_{11} & \dot{\kappa}_{22} & 2\kappa_{12} \end{bmatrix} \quad \dot{\boldsymbol{\gamma}} = \begin{bmatrix} \dot{\gamma}_{1} & \dot{\gamma}_{2} \end{bmatrix} \tag{77}$$

Substitution of eq. (76) into the discretized form of the Hu-Washizu functional and subsequent variations with respect to the independent field variables, lead to the formulation of the tangent stiffness matrix for the layered element.

Computation of the elemental internal forces is attained by numerically or analytically integrating the stresses in the concrete and steel layers.

$$n_{c}^{\alpha\beta} = \int_{-t/2}^{+t/2} \sigma_{c}^{\alpha\beta} d\theta^{3}, \quad \alpha,\beta = 1,2 \tag{78}$$

$$m_{c}^{\alpha\beta} = \int_{-t/2}^{+t/2} \theta^{3} \sigma_{c}^{\alpha\beta} d\theta^{3} \qquad q_{c}^{\alpha} = \int_{-t/2}^{+t/2} \left[1 - \left(\frac{2\theta^{3}}{t} \right)^{2} \right] \sigma_{c}^{\alpha 3} d\theta^{3} \tag{79}$$

$$n_{s}^{\alpha\alpha} = \sum_{i=1}^{N} \rho_{i} t \sigma_{si}^{\alpha\alpha} \qquad m_{s}^{\alpha\alpha} = \sum_{i=1}^{N} \rho_{i} t (\theta_{i}^{3}) \sigma_{si}^{\alpha\alpha} \tag{80}$$

4. NUMERICAL EXAMPLES

Three characteristic test examples are analyzed using the proposed approach. The results of the finite element models include prediction of the ultimate load and the corresponding mode of failure, force-displacement curves up to failure and cracking

patterns. The incremental approximation of the nonlinear problem is implemented using a modified Newton-Raphson iterative procedure. The tangent stiffness matrix of the structure is revised in the first iteration of each load increment and is maintained constant during subsequent iterations within the increment. The size of the load increments is constant throughout the analysis and the total number of load steps ranges from 10 to 15, depending on the problem. The convergence criterion for the termination of the iterative procedure is as follows

$$\left\|\Delta \boldsymbol{u}_i^n\right\| \;/\; \left\|\sum_{k=1}^{i} \Delta \boldsymbol{u}_k^n\right\| \le DTOL \tag{81}$$

whereas $\|\boldsymbol{x}\| = (\boldsymbol{x}^T \boldsymbol{x})^{1/2}$ is the Euclidean norm of vector $\mathbf{x}$, $\Delta \mathbf{u}_k^n$ is the incremental change of the displacement vector at iterative cycle i and $\sum_{k=1}^{i} \Delta \mathbf{u}_k^n$ is the total incremental change of the displacements within load increment n. The convergence tolerance DTOL is taken equal to 0.02. Failure is assumed to occur if the convergence tolerance is not satisfied within 40 iterations. In case of nonconvergence, the results are examined in order to determine the failure mode of the structure.

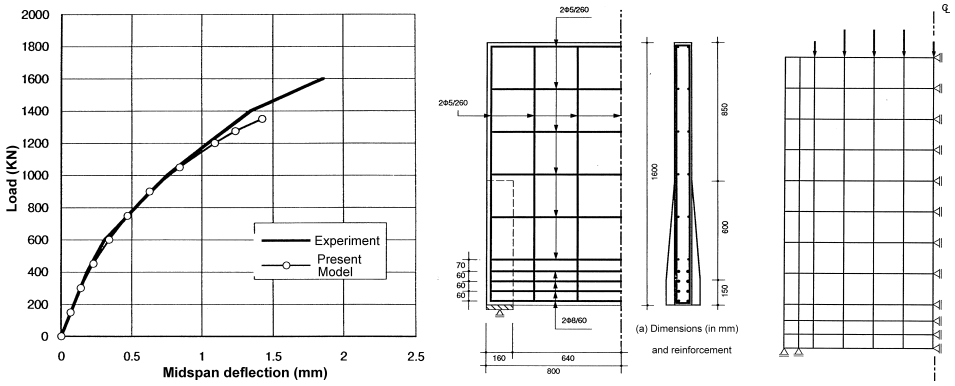

Fig. 2. Reinforced concrete deep beam: Finite element mesh and comparison of results'

A reinforced concrete deep beam tested by Leonhardt and Walther [26] has been investigated. The 100 mm thick simply supported beam has a span of 1600 mm and a total depth of 1600 mm. It is subjected to a constant load acting along the top edge. The reinforcement pattern of the beam is shown in Fig. 2. The material properties for the concrete and for the reinforcing steel are $f_c = 29.6$ MPa, $\varepsilon_0 = 2‰$, $E_{c0} = 29.6$ GPa, $f_{ct} = 2.87$ MPa, $v = 0.2$ and $f_y = 415$ MPa, $E_s = 206$ GPa, $E_{sp} = 4.6$ GPa, respectively. Taking advantage of the symmetry, only half of the beam is discretized using 66 plane stress elements (Fig. 2). The predicted response for the midspan deflection versus total load is plotted, together with the observed response in Fig. 2. There is a good agreement between the results of the proposed approach and of the experimental measurements. Nevertheless, the failure load is underestimated (1350 KN versus 1600 KN, approximately). This discrepancy is due to the smeared representation of cracking which results to an artificially expanded cracking zone at ultimate load level. The numerical model accurately predicts the

failure mode of the beam, which is due to yielding of the horizontal reinforcement at the support region.

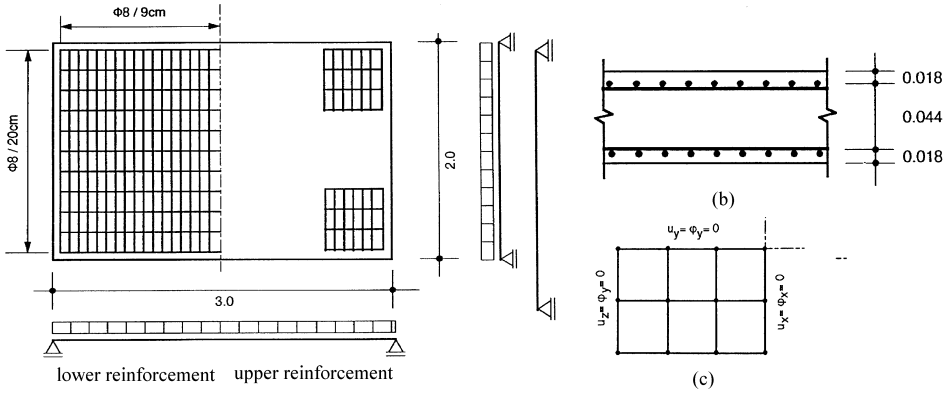

Fig. 3. Simply supported reinforced plate: Dimensions and reinforcement

A simply supported rectangular plate of dimensions ($200 \times 300 \times 8$ cm) tested by Franz [27] is analyzed (Fig. 3). The slab was reinforced with 9×20 cm wire mesh of diameter 8 mm. Material properties for the concrete are $f_c = 26.5$ MPa, $\varepsilon_0 = 2.2‰$ $E_{c0} = 24$ GPa, $f_{ct} = 26.7$ MPa, and $\nu = 0.20$. Reinforcing steel is treated as an ideally elastoplastic material with $f_y = 420$ MPa and $E_s = 200$ GPa. Due to double symmetry, only one quarter of the slab is analyzed. Two alternative approximations for the tension stiffening of concrete are employed. Model M1 utilizes a decaying function according to eq. (42), while model M2 incorporates the relationships proposed in [29]:

$$\sigma_{c1} = f_{ct} \text{ for } \varepsilon_{ct} < \varepsilon_1 < 2\varepsilon_{ct}\,, \quad \sigma_{c1} = f_{ct}\left(\frac{2\varepsilon_{ct}}{\varepsilon_1}\right)^{0,4} \text{ for } \varepsilon_1 > 2\varepsilon_{ct} \qquad (82), (83)$$

The load-displacement curves for the midpoint are presented in Fig. 4. Model M2 approximates the experimental curve more accurately at early loading stages. The differences between the two models decrease as load increases since the contribution of tension stiffening to overall stiffness is rather negligible at higher load levels. Both models predict an ultimate load of 55 KN/m^2. The test results were measured only up to a load of about 52 KN/m^2 in order to save the test equipment in case of a sudden failure. The crack distribution at the lower side of the test specimen and the analytically predicted crack pattern are compared in Fig. 4.

The structural behavior of precast reinforced concrete pipes with circular cross section was experimentally investigated by Heger et al. [28]. A number of pipe segments with variable material properties and reinforcement patterns were subjected to the standard three-edge bearing test up to collapse load. The experimental procedure included the determination of cracking and ultimate load, measurements of change in pipe diameter and recording of crack locations. The proposed finite element model is used to analyze the behavior of the pipe specimen I-2 tested in [28]. The specimen is 4 ft long, the inner diameter is 48 in and the thickness of the pipe wall is 5 in. The reinforcement consists of

two welded wire meshes in both the inner and outer faces of the pipe wall. Steel percentages in the circumferential direction are 3.98‰ and 2.9‰ for the inner and the outer wire mesh, respectively. Material properties for concrete are $E_{c0} = 4.6 \cdot 10^6$ psi, $f_c = 5930$ psi, $\varepsilon_0 = 2.6‰$, $f_{ct} = 532$ psi, $\nu = 0{,}2$ and for the reinforcing steel $E_s = 30 \cdot 10^6$ psi, $E_{sp} = 30 \cdot 10^4$ psi, $f_y = 86000$ psi and $\varepsilon_{su} = 10‰$. Due to symmetry, one eighth of the pipe is discretized using a 2×8 mesh of shell elements. Finally, along the crown of the pipe specimen a constant load is applied. The numerically obtained curve for pipe deflections versus total load (Fig. 5) demonstrates that the proposed model may satisfactorily describe the deformational behavior of the pipe. The calculated failure load of 52000 lb compares favorably with the measured failure load of 53400 lb. Furthermore, the model correctly predicts the pipe failure mode which is caused by yielding of the inner hoop reinforcement at the crown.

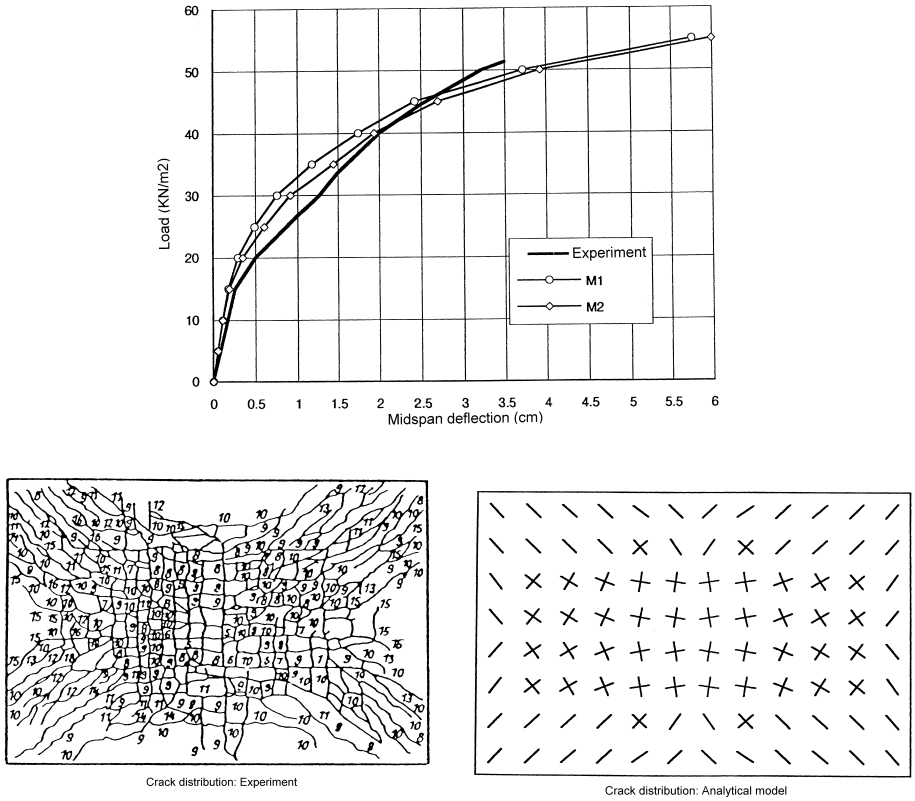

Fig. 4. Simply supported R/C plate: Comparison of results

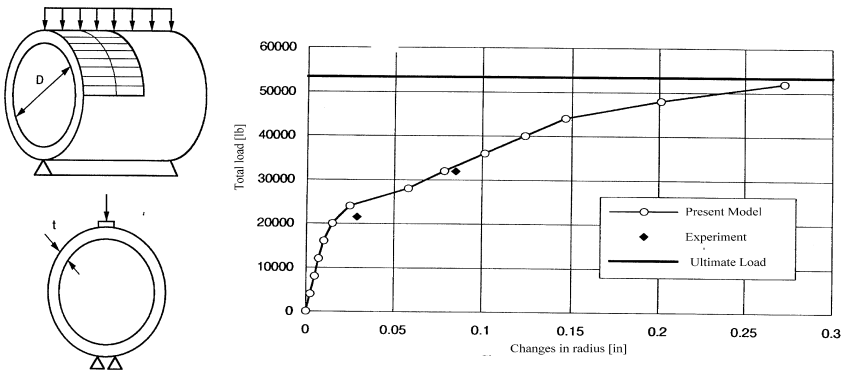

Fig. 5. Precast reinforced concrete pipe

REFERENCES

1. G. Wempner, D. Talaslidis, C. M. Hwang, *A simple and efficient approximation of shells via finite quadrilateral elements*, ASME, J. Appl. Mech., **49,** 115-120 (1982).
2. A. Tokatlidis, *Development of C^o quadrilateral finite elements for the nonlinear analysis of reinforced concrete plates and shells*, Ph. D. Thesis, Aristotle University Thessaloniki (1996).
3. F. Vecchio, M. P. Collins, *The response of reinforced concrete to in-plane shear and normal stresses*, Publ. 82-03, University of Toronto, Dept. Civil Engng. (1982).
4. S. B. Bhide, M. P. Collins, *Reinforced concrete elements in shear and tension*, Publ. 87-02, University of Toronto, Dept. Civil Engng. (1987).
5. H. Stolarski, T. Belytschko, S.-H. Lee, *A review of shell finite elements and corotational theories*, Computational Mechanics Advances, **2**, 125-212 (1995).
6. D. Talaslidis, G. Wempner, *A. simple finite element for elastic-plastic deformations of shells*, Comp. Meth. Appl. Mech. Engng., **34**, 1051-1064 (1982),.
7. D. Talaslidis, G. Wempner, *The linear isoparametric triangular element: Theory and application*, Comp. Meth. Appl. Mech. Engng., **103**, 375-397 (1993).
8. C. Karakostas, D. Talaslidis, *Triangular C^o bending elements based on the Hu-Washizu principle and orthogonality conditions*, Int. J. Num. Meth. Engng., **36**, 181-200 (1993).
9. D. Talaslidis and I. Sous, *A discrete Kirchhoff triangular element for the analysis of thin stiffened shells*, Comp. Struct., **43**, 663-674 (1992).
10. G. Wempner, D. Talaslidis, *Mechanics of solids and shells*: *foundations*, CRC-Press, to appear (2000).
11. H. Kupfer, K. Gerstle, *Behavior of concrete under biaxial stresses*, ASCE J. Struct. Div., **99**, 853-866 (1973).
12. S. Balakrishnan, D. Murray, *Concrete constitutive model for NLFE analysis of structures*, ASCE J. Struct. Div., **114**, 1449-1466 (1988).
13. Z. P. Bazant, *Comment on orthotropic models for concrete and geomaterials*, ASCE J. Engng. Mech. Div., **109**, 849-865 (1983).
14. D. Murray, K. Chitnuyanondth, K. Rijub-Agha, C. Wong, *Concrete plasticity theory for biaxial stress analysis*, ASCE J. Engng. Mech. Div., **105**, 989-1006 (1979).
15. S. Hsieh, E. Ting, W. Chen, *Applications of plastic-fracture model to concrete structures*, Comp. Struct., **28**, 373-393 (1988).
16. Z. P. Bazant, C. L. Shieh, *Hysteretic fracturing endochronic theory for concrete*, ASCE J. Struct. Div., **106**, 929-950 (1980).
17. H. Grootenboer, S. Leijten, J. Blaanwenraad, *Numerical models for reinforced concrete structures in plane stress*, Heron, **26**, (1986).
18. G. Hofstetter, H. A. Mang, *Computational mechanics of reinforced concrete structures*, Vieweg (1995).
19. R. de Borst, P. Nauta, *Non-orthogonal cracks in a smeared finite element model*, Engng. Comput., **2**, 35-

46 (1985).
20. L. N. Adeghe, M. P. Collins, *A finite element model for studying reinforced concrete detailing problems*, Publ. 86-12, Univ. of Toronto, Dept. Civil Engng. (1986).
21. M. Crisfield, J. Wills, *Analysis of R/C panels using different concrete models*, ASCE J. Mech. Div., **115**, 578-597 (1989).
22. P. H. Feenstra, R. de Borst, *Aspects of robust computational modelling for plain and reinforced concrete*, Heron, **38**, Delft, (1993).
23. M. A. Polak, F. J. Vecchio, *Nonlinear analysis of reinforced concrete shells*, ASCE J. Struct. Engng., **119**, 3439-3462 (1993).
24. R. G. Selby, F. J. Vecchio, *A constitutive model for analysis of reinforced concrete solids*, Can. J. Civ. Engng., **24**, 460-470 (1997).
25. ENV 1992-1-1:1991. *Eurocode 2: Design of concrete structures. Part 1: General rules and rules for buildings*.
26. F. Leonhard, R. Walther, *Wandartige Traeger*, *Deutscher Ausschuss fuer Stahlbeton*, Heft 178 (1966).
27. G. Franz, *Ueber die Beanspruchung der Bewehrung von kreuzweise bewehrten vierseiting frei drehbar gelagerten Rechtechplatten aus Stahlbeton*, Untersuchungs- bericht des Instituts fuer Beton und Stahlbeton, Karlsruhe (1970).
28. F. Heger, E. Nawy, R. Saba, *Structural behavior of circular concrete pipe reinforced with welded wire fabric*, ACI Jounal, (1963).
29. J. Izumo, H. Shin, K. Maekawa, H. Okamura, *An analytical model for R/C panels subjected to in-plane stresses*, Concrete Shear in Earthquake, Elsevier Appl. Science, 206-215.

NELINEARNA ANALIZA KONAČNIH ELEMANATA R/C LJUSKI

Demosthenes G. Talaslidis, Aristotle Ch. Tokatlidis

Ovaj rad je usredsređen na razvoj i implementaciju odgovarajuće formulacije konačnog elementa i materijalnog modela makronivoa za efikasnu i pouzdanu nelinearnu analizu pojačanih konkretnih (re/inforce concrete R/C) ljuskastih struktura.U tom cilju formulacija elementa je predstavljena na osnovu Hu-Washizu-ovog principa. Nezavisne aproksimacije pomeranja (bilinearne), napona i naprezanja (konstantni po delovima) obezbeđuju konzistentni mehanizam za opisivanje progresivnih promena svojstava materijala kroz element. Sem toga, ponovna ocena koeficijenata krutosti i unutrašnjih sila, kao i korekcija neravnoteže u uzastopnim inkrementima postaju vrlo jednostavne, čime se ostvaruje smanjenje vremena izračunavanja. Korišćeni model materijala zasniva se na pretpostavkama "Modifikovane teorije kompresije polja". Ovaj model zajedno sa slojevitim pristupom može na ekspeditivan i ekonomičan način predvideti u globalnom smislu ukupno konačno ponašanje opterećenja. Test primeri su analizirani korišćenjem predloženog pristupa i izvršena su upoređivanja sa merenjima dobijenim na osnovu eksperimentalnih istraživanja.